Tetrahedral potentials and lack-of-inversion symmetry for donors in silicon

T. G. Castner, Jr.
Department of Physics and Astronomy, University of Rochester, Rochester, New York 14627, USA
(Received 15 January 2009; published 20 May 2009)

The extensive electron-nuclear double resonance data of Hale and Mieher for P-, As-, and Sb-doped Si and the comprehensive multiband calculation of Ivey and Mieher employing only a spherical potential $U(r)$ suggests four inversion-related pairs [(224), (224)], [(444), (444)], [(228), (228)], and [(2212), (2212)] have been associated with the shells $[M,L]$, $[H,O]$, $[I,P]$, and $[S,T]$. An alternative explanation is provided resulting from tetrahedral potentials of the form $V_{\text{tet}}(\mathbf{r})=V_t\ xyx/(r^2+b^2)^{7/2}$ and a corresponding wave function $\psi_{\text{tet}} \propto -xyz\ [C_1 \exp(-r/\lambda_1)+C_2 \exp(-r/\lambda_2)]$ with $C_1 \gg C_2$ and $\lambda_2 \sim 4\ \lambda_1$ (for P donor). ψ_{tet} leads to a giant octupole moment for the donors dominated by $C_2 \exp(-r/\lambda_2)$. Excellent agreement is obtained for P, good agreement for As, and less satisfactory agreement for Sb. $V_{\text{tet}}(\mathbf{r})$ originates from the donor **E**-field-induced electric dipoles $\mathbf{p}_i$ at the covalent bond sites [first nearest-neighbor (nn), second nn, and third nn] as calculated by Harrison. Reasons are provided why the inversion-related pairs cannot be explained by a spherical potential $U(r)$. These results provide strong support for the assignments by Ivey and Mieher of the four inversion-related pairs. The interest in donors in Si as possible quantum bits has led to interest in the Stark effect from external electric fields. $V_{\text{tet}}(\mathbf{r})$ and the associated $\psi_{\text{tet}}(\mathbf{r})$, resulting from an "internal Stark effect," are a general feature for impurities with T_d symmetry in semiconductors.

DOI: 10.1103/PhysRevB.79.195207 PACS number(s): 76.70.Dx

I. INTRODUCTION

In the numerous studies of shallow donors in *n*-type Si, the emphasis has been on the energy levels[1] and the optical transitions[2] (electric dipole) between the various bound levels. In almost all these studies. the potential employed has been a spherical potential $V(r)=-[e^2/\varepsilon_h r+V_{\text{cc}}(r)]$ where ε_h is the host static dielectric constant. $V_{\text{cc}}(r)$ is the donor-dependent central-cell potential important for $r<2.35$ Å which plays an important role in the substantial corrections to the $1s$-A_1 energies and to the strong coupling between the six Δ_1 minima. Faulkner[3] calculated the energy levels of the lowest $6S$ states and the lowest $18P$ states using only the Coulombic potential. The actual symmetry for the substitutional donors is tetrahedral (T_d group) and there will be a potential $V_{\text{tet}}=xyz\ f(r)$ which is not well understood[4] and was mentioned by Ning and Sah[5] but then neglected. V_{tet} will have a negligible effect on the ground-state (GS) energy $E_{1s\text{-}A1}$ but can affect the GS wave function ψ_{GS} by introducing a component [A_1 representation] lacking inversion symmetry that arises from $n \geq 4$ f ($\ell=3$ and $m=\pm 2$) hydrogenic-like functions. Inversion-related shell pairs have been observed in the electron-nuclear double resonance (ENDOR) data of Hale and Mieher[6] (HM). Most of the experimental shells were not related to specific lattice sites until the comprehensive multiband theory of Ivey and Mieher[7] (IM) which identified most of the experimental shells with lattice sites. In particular, IM identified the inversion-related pairs [H (444), O (444)], [M (224), L (224)], [I (228), P (228)], and [S (2212), T (2212). IM made this identification neglecting V_{tet}, considering only a spherical $V(r)$. This paper considers the lack-of-inversion symmetry (LOIS) in ψ_{GS} to arise from V_{tet} and explains the donor dependence of LOIS more satisfactorily than the IM approach. IM emphasized some of the problems with effective-mass theory (EMT), but this work suggests EMT is better than implied by the IM approach. The origin of V_{tet}, its donor dependence, and the relation to the covalent bond will be considered.

$V_{\text{tet}}(\mathbf{r})$ originates from the polarization of the host covalent bonds by the internal donor electric field **E**, and for a given host can be viewed as an internal Stark effect, but with no change of the local symmetry (A_1 for the GS ψ). Kane's[8] proposal to utilize the nuclear spins of ^{31}P donors in Si as qubits rejuvenated interest in donor wave functions and how they are tuned by an external electric fields using metallic gates. This external Stark effect ($H_{\text{pert}}=eEz$ and T_2 symmetry) has been a key approach in tuning donor wave functions and ^{31}P and ^{29}Si hyperfine interactions. Furthermore, electrically detected magnetic resonance[9] (EDMR), optically detected (Faraday rotation) of electron spins in semiconductor quantum wells (QWs), and g-tensor modulation resonance[10] (g-TMR) for a single spin bound to a donor are all examples of the role of electric fields in the rapidly expanding field of spintronics.[11]

II. TETRAHEDRAL POTENTIALS

For donors in Si, the symmetry is tetrahedral (T_d group) and the potential seen by the donor electron must belong to the A_1 representation. The tetrahedral potential $V_{\text{tet}}(\mathbf{r})$ can take the form

$$V_{\text{tet}}(\mathbf{r}) \approx V_t xyz/(r^2+b^2)^{7/2}, \tag{1}$$

where $b \approx \sqrt{3}a/8$ ($a=5.43$ Å for Si) is the distance to the nearest-neighbor (nn) covalent bond. The tetrahedral potential V_{tet}, which can arise either from four charges or four electric dipoles, (pointed out from the donor) was placed on the four corners of a tetrahedron. The exponent 7/2 is the same for either charges or electric dipoles. V_{tet} is short range and falls off like r^{-4} for $r \gg b$, which is the expected behavior for an octupole moment.

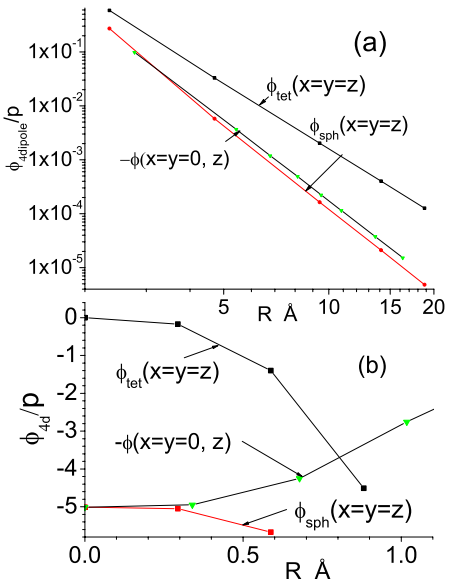

FIG. 1. (Color online) (a) $\varphi_{4\text{dipole}}/p$ vs R for the various components $\varphi_{\text{tet}}(x=y=z)$, $\varphi_{\text{sph}}(x=y=z)$, and $-\varphi(x=y=0,z)$ [(001) axis]. $\varphi_{\text{tet}}(x=y=z)$ falls off as R^{-4} [$\varphi_{\text{sph}}(x=y=z)$ as R^{-5}] for $R>8|\mathbf{r}_i|$ =9.4 Å. (b) These components for $R<|\mathbf{r}_i|$ inside the "cage" of four dipoles. Note that $\varphi_{\text{tet}}(x=y=z)$ changes sign between $R<|\mathbf{r}_i|$ and $R>2|\mathbf{r}_i|$.

The potential from four charges will be $\varphi_{4q}=(q/\varepsilon_h)\Sigma_{i=1}^{4}1/|\mathbf{r}-\mathbf{r}_i|$, where $\mathbf{r}_1=(a/8)[\mathbf{i}+\mathbf{j}+\mathbf{k}]$, $\mathbf{r}_2=(a/8)[\mathbf{i}-\mathbf{j}-\mathbf{k}]$, $\mathbf{r}_3=(a/8)[-\mathbf{i}+\mathbf{j}-\mathbf{k}]$, and $\mathbf{r}_4=(a/8)[-\mathbf{i}-\mathbf{j}+\mathbf{k}]$. Evaluating $\varphi_{4q}(x=y=z)$, one can show $\varphi_{4q,\text{sph}}(x=y=z)=\frac{1}{2}[\varphi_{4q}(x=y=z)+\varphi_{4q}(-x=-y=-z)]$ and $\varphi_{4q,\text{tet}}(x=y=z)=\frac{1}{2}[\varphi_{4q}(x=y=z)-\varphi_{4q}(-x=-y=-z)]$. Even though $\varphi_{4q,\text{tet}}(x=y=z)\propto xyz/(r^2+b^2)^{7/2}$ for $r\gg b$ has the right dependences, one finds $\varphi_{4q,\text{sph}}(x=y=z)\propto q/r$ for $r\gg b$. Thus, the four charges model is unacceptable because it leads to a long-range repulsive Coulombic potential in addition to the standard attractive potential $e/\varepsilon_h r$. Furthermore, for q negative (as expected for the valence bond charge), one has the wrong sign for φ_{4q} and ψ_{tet} that is required to explain the ENDOR data.

Alternatively, the electrostatic potential from four nn dipoles pointed outward from the donor along the four $\mathbf{r}_i$ is given by

$$\varphi_{4\text{dipole}}=(1/\varepsilon_h)\sum_{i=1}^{4}\mathbf{p}_i\cdot(\mathbf{r}-\mathbf{r}_i)/|\mathbf{r}-\mathbf{r}_i|^3, \tag{2}$$

where $\mathbf{r}$ is measured from the donor origin. Using the same definitions as above for $\varphi_{4\text{dipole,tet}}(x,y,z)$ and $\varphi_{4\text{dipole,sph}}(x,y,z)$, one calculates these quantities along the (111) axis for $R=|\mathbf{r}|>2$ Å. The results are for φ_{4d}/p, where p is the magnitude of the induced dipole moment associated with the nn covalent bond, are shown in Fig. 1(a). $\varphi_{4d,\text{tet}}(x=y=z)/p$ falls off very closely as r^{-4} for $R>8|\mathbf{r}_i|$, while $\varphi_{4d,\text{sph}}(x=y=z)/p$ falls off as r^{-5} for $R>8|\mathbf{r}_i|$. The significant result is that $\varphi_{4d,\text{sph}}\ll\varphi_{4d,\text{tet}}$ for large R when the four dipoles are nearly equidistant from the field point. At the (444) site (shell O) where $R=9.404\,7$ Å $\varphi_{4d,\text{tet}}/\varphi_{4d,\text{sph}}\approx 12.4$. Since $\Sigma_{i=1}^{4}\mathbf{p}_i=0$ the dipolar component of $\varphi_{4\text{dipole}}$ is negligible at large R. Figure 1(a) also shows $-\varphi_{4d}(x=y=0,z)$ along the cubic axis (001). Along this axis $\varphi_{4d,\text{tet}}$ is zero, but there can be a quadrupolar contribution of the form $(x^2+y^2-2z^2)/(r^2+b^2)^{5/2}$ because on this axis there are two pairs of equidistant dipoles with two different distances for each finite z. Also shown in Fig. 1(b) are the potentials inside the tetrahedral "cage" for $0<R<1$ Å. $\varphi_{4d,\text{tet}}(x=y=z)/p$ starts at 0 and increases negatively as r^3 for $r<b$. $\varphi_{4d,\text{sph}}/p$ starts at −5.012 and becomes more negative because along (111), one is approaching a dipole and a singularity as $R\rightarrow|\mathbf{r}_1|$, but the singularity can be avoided along the (11$\underline{1}$) axis. $\varphi_{4d}(x=y=0,z)$ decreases from −5.012 at $R=0$ to smaller values. Note that some components of $\varphi_{4\text{dipole}}$ change sign from inside the dipole cage to outside. The primary concern of this paper is $V_{\text{tet}}(\mathbf{r})$, $\psi_{\text{tet}}(\mathbf{r})$, and the explanation of the LOIS in the ENDOR data; however it should be noted that the $\varphi_{4d,\text{sph}}(r)$ term may have some effect on the radial wave function and might affect the GS energy. To proceed further, we need the magnitude of p in order to obtain the magnitude of $V_{\text{tet}}(\mathbf{r})$.

In the presence of a radial electric field E_r from the donor, there is an induced dipole moment associated with the covalent bond obtained by Harrison[12] given by

$$\mathbf{p}=e\gamma\mathbf{d}(V_3+e\gamma\mathbf{d}\cdot\mathbf{E}/2)/[V_2^2+(V_3+e\gamma\mathbf{d}\cdot\mathbf{E}/2)^2]^{1/2}, \tag{3}$$

where $\mathbf{d}$ is the atom-to-atom vector [$\mathbf{d}_1=(a/4)(\mathbf{i}+\mathbf{j}+\mathbf{k})$, $\mathbf{d}_2=(a/4)(\mathbf{i}-\mathbf{j}-\mathbf{k})$, $\mathbf{d}_3=(a/4)(-\mathbf{i}+\mathbf{j}-\mathbf{k})$, and $\mathbf{d}_4=(a/4)(-\mathbf{i}-\mathbf{j}+\mathbf{k})$ for the nn bonds] V_2 is the covalent energy, V_3 is the polar energy, and $e\gamma\mathbf{d}\cdot\mathbf{E}/2$ is induced dipole energy. γ is a numerical scaling factor [Si, $\gamma=1.40$] which depends on the Z of the two atoms in the covalent bond. For the second and third nn bonds $V_3=0$, $E_r\approx e/\varepsilon_h r^2$ and $\mathbf{E}\cdot\mathbf{d}=E_r d\cos\theta$. For the four nn dipoles $\cos\theta=1$, while for the second nn bonds $\cos\theta=0.685$, and for the third nn bonds $\cos\theta=0.889$. For Si:P V_3 is small compared to $e\gamma\mathbf{d}\cdot\mathbf{E}/2$.

III. ψ_{tet} AND THE FERMI CONTACT HYPERFINE INTERACTION

The potential [Eq. (1)] couples ψ_{GS} to hydrogeniclike states with $n\geq 4$, $\ell=3$, $m=\pm 2$ [$xyz=r^3\sin^2\theta\cos\theta(e^{2i\varphi}-e^{-2i\varphi})/2i$]. The matrix elements $\langle n3|V_{\text{tet}}||\psi_{\text{GS}}\rangle$ are very small [$\langle 43|V_{\text{tet}}|\psi_{\text{GS}}\rangle<8\times10^{-6}$ meV] compared to $E_{1S\text{-}A1}-E_{n\ell=3,\ m=\pm2}$ and decrease with n as $n\rightarrow\infty$. ψ_{tet} takes the form

$$\psi_{\text{tet}}=xyz\sum_{4}^{\infty}A_{n,\ell=3}[\langle n,\ell=3|V_{\text{tet}}|1S\text{-}A_1\rangle/(E_{1S\text{-}A1}-E_{n,\ell=3,m=\pm2})]e^{-\alpha r/n}L_{n-4}^{7}(2\alpha r/n), \tag{4}$$

where $L_{n-4}^{7}(2\alpha r/n)$ is a Laguerre polynomial, $A_{n,\ell=3}$ is a normalization coefficient, and the ratio $\langle\ \rangle/(\ )$ falls off slowly with n. One must perform the sum in Eq. (4) from $n=4$ to ∞ Using the generating function result[13] for associated Laguerre polynomials, this sum yields the approximate result

$$\psi_{\text{tet}}\sim -C_1'xyze^{-r/\lambda}\sim -C_1(xyz/a^3)e^{-r/\lambda}, \tag{5}$$

where $\lambda\ll 4a^*$ ($4a^*$ the Bohr radius for $n=4$). λ will be viewed as an empirical parameter. If there was a second

contribution to V_{tet} from, for example, more distant dipoles then the generalization of Eq. (5) would be $(xyz/a^3)[C_1 \exp(-r/\lambda_1)+C_2 \exp(-r/\lambda_2)]$ where $C_2 \ll C_1$. ψ_{tet} is negative in the positive octant ($x>0$, $y>0$, and $z>0$). Employing a modified Eq. (1) from Castner[14] (CA) of the form

$$\psi_d = N_d^{1/2}\{[\ ]_{is} + [\ ]_{KL}\psi_{tet}\}, \tag{6}$$

where $[\ ]_{is}$ includes all terms from Δ_1 and subsidiary minima in Eq. (1) appropriate for even sites (this excludes A_{XU} contributions which occur only for odd sites and the $I^I_\Delta = F^I_x \sin k_0x + F^I_y \sin k_0y + F^I_z \sin k_0z$ term introduced by IM). As a result $[\ ]_{is}$ exhibits inversion symmetry. $[\ ]_{KL} = (2/\sqrt{6})[\cos k_0x + \cos k_0y + \cos k_0z]$ is the Kohn-Luttinger (KL) sum over the six Δ_1 minima and Eq. (6) implies ψ_{tet} is the same for each Δ_1 minimum which means the valley mass anisotropy is neglected for ψ_{tet}. Using $a_{hpf}(nnm) \propto |\psi_d(nnm)|^2$, $\Delta a_{hpf}(nnm) = a_{hpf}(\underline{nnm}) - a_{hpf}(nnm)$, and $a_{hpf,av}(nnm) = [a_{hpf}(\underline{nnm}) + a_{hpf}(nnm)]/2 \propto N_d[nnm]^2_{is}$, one can derive an expression for $\Delta a_{hpf}/a_{hpf}$ of the form

$$\Delta a_{hpf}(nnm)/a_{hpf,av}(nnm) = -4\{[nnm]_{KL}/[nnm]_{is}\}\psi_{tet}(nnm), \tag{7}$$

where a negligible term $[\ ]^2_{KL}|\psi_{tet}(nnm)|^2$ has been ignored in $a_{hpf,av}(nnm)$. The experimental ratios $\Delta a_{hpf}(nnm)/a_{hpf,av}(nnm)$ are directly determined from the values for the four LOIS related pairs in Table I. $[nnm]_{KL}$ is calculated and $[nnm]_{is}$ is determined from $a_{hpf,av}(nnm)$, where N_d is determined from CA.[14] $[nnm]_{KL}$ and $[nnm]_{is}$ can be either positive or negative, but both have the same sign. Hence Eq. (7) permits a direct determination of $\psi_{tet} = -(xyx/a^3)[C_1 \exp(-r/\lambda_1)+C_2 \exp(-r/\lambda_2)]$. It is unrealistic to calculate reliable values of the parameters (C_1, λ_1) and (C_2, λ_2) from first-principles theory. It is more realistic to use the data for the four LOIS site pairs to determine values of (C_1, λ_1) and (C_2, λ_2). This approach allows us to characterize ψ_{tet} and obtain information on the magnitude of contributions to $V_{tet}(\mathbf{r})$. It is not obvious that ψ_{tet} can be represented by just two terms and four parameters, however, that turns out to be the case for the P donor, which has the simplest valence-band covalent nn bond.

IV. INVERSION-RELATED SHELL ENDOR DATA AND IVEY-MIEHER RESULTS

Table I shows the Fermi contact constants $a/2$ for the inversion-related sites as identified by IM in addition to the inversion-related differences and averages. The calculated values of IM and the IM (with F^I and $G=0$) are also shown for comparison with the data. The quantities F^I and G are defined in Eqs. (44) and (45) in IM and the numerical values are given in Table II. The most striking result for shells H and O is the donor anomaly $a/2(\text{As}) > a/2(\text{Sb}) > a/2(\text{P})$ but with the difference $(H\text{-}O)$ largest for P and smallest for Sb.

This donor anomaly is a significant clue as to the origin of the inversion difference between $\psi_d(\underline{xxz})$ and $\psi_d(xxz)$. The IM calculation contains $F^I_x \sin(k_0x)$ terms, etc. [see Eq. (46) in IM] that result because $u_k(\mathbf{r})$ is not real off the principal $\Gamma\Delta X$ axes. However, Table I shows the IM difference values $[H\text{-}O]$ and $[M\text{-}L]$ which are substantially larger than the experimental values and that the IM (G and $F^I=0$) average values are in better agreement with the experimental. results. Removing these sine terms by setting $F^I=0$ does not remove the difference between (nnm) and (nnm) values, raising questions about the origin of the lack-of-inversion compo-

TABLE I. Inversion-related Fermi contact constants, differences, and averages (in KHz).

	Expt.			IM			IM (G and $F^I=0$)		
Shell site	As	P	Sb	As	P	Sb	As	P	Sb
H ($\underline{444}$)	801	689	703	943	787	713	805	683	626
O (444)	739	598	670	775	652	593	765	654	598
Difference	62	91	33	168	135	120	40	29	28
Average	770	643.5	686.5	859	719.5	653	789	668.5	612
M ($\underline{224}$)	777	612	559	819	612	576	778	590	510
L (224)	741	582	525	716	537	502	730	555	479
Difference	36	30	34	103	75	74	48	35	31
Average	759	597	542	764.5	574.5	539	754	572.5	499.5
I ($\underline{228}$)	718	685	643	646	589	556	778	590	510
P (228)	696	662	629	627	573	541	730	555	479
Difference	22	23	14	19	16	15	48	35	31
Average	707	673.5	636	636.5	581	548.5	754	572.5	494.6
S ($\underline{2212}$)	377	410	425	411	424	422	419	429	425
T (2212)	364	398	425	401	415	412	430	439	434
Difference	13	12	0	10	9	10	−11	−10	−9
Average	370.5	404	425	406	419.5	417	424.5	434	429.5

nent in the IM ψ. One also notes large differences between the IM values $[I\text{-}P]$ and $[S\text{-}T]$ and the IM (G and $F^I=0$) $[I\text{-}P]$ and $[S\text{-}T]$ values. It is clear the IM calculation contains several different LOIS contributions. Inspection of the IM envelope functions in Table II shows that Re $F_x(\underline{\text{nnm}}) \neq$ Re F_x(nnm) and Re $F_z(\underline{\text{nnm}}) \neq$ Re F_z(nnm). This shows that the IM ψ exhibits LOIS even for $F_x^I=F_z^I=0$. The origin of this inversion asymmetry in the real part of the envelope functions is not obvious and certainly not consistent with the EM theory envelope functions even for the subsidiary minima considered recently by CA (Ref. 10) for the odd sites. One should emphasize that the IM potential $U(\mathbf{r})$ has inversion symmetry

V. FITTING ANALYSIS TO DETERMINE ψ_{tet}

The experimental data for four inversion-related sites (data in Table I) can be employed to determine the four parameters (C_1, λ_1) and (C_2, λ_2). The first term $C_1 \exp(-r/\lambda_1)$ arises from the nn dipoles, while the second term $C_2 \exp(-r/\lambda_2)$ comes from the second and third nn dipoles, leading one to expect $\lambda_2 \sim 4\lambda_1$ and $C_1 \gg C_2$. Four equations of the form

$$K_i = C_1 \exp(-R_i/\lambda_1) + C_2 \exp(-R_i/\lambda_2), \quad i = 1 \text{ to } 4. \tag{8}$$

R_i varies from 6.6503 6 Å (224) to 16.7364 Å (2212). For the two smaller R_i ($i=1,2$), the first term dominates, while for $i=4$ (2212) the second term dominates. Since the form of K_i is similar for each i, it is not so easy to solve Eq. (8) for the four parameters. The procedure for evaluating the parameters was to choose a λ_1 and obtain $K_i \exp(R_i/\lambda_1) = C_1 + C_2 \exp[R_i/(1/\lambda_1 - 1/\lambda_2)]$. One chooses a λ_2 and solves each pair ($i=1,2$) and ($i=3,4$) for C_1 and C_2. In general, one obtains two values of C_1 and two values of C_2. Next one tries new values of λ_2 until one finds a new $C_1(i=1,2)=C_1(i=3,4)$. In general, one finds $C_2(i=1,2)$ larger than $C_2(i=3,4)$, and one chooses the smaller value because it is the dominant term for $i=4$. One then iterates the entire process and obtains new values of $C_1(i=1,2)=C_1(i=3,4)$. One then plots $C_1 \exp(-R_i\lambda_1)=K_i - C_2 \exp(-R_i/\lambda_2)$ versus R_i to check for good exponential behavior (see Fig. 2) and to find a final value of λ_1 (and λ_2). Finally, one calculates $\Delta a_{\text{hpf}}(\text{nnm})/a_{\text{hpf,av}}(\text{nnm})$ and varies C_1 and C_2 to minimize the rms value after summing over the four sites. Table II shows the results of this empirical fit for the P donor and calculated and experimental values of $\Delta a_{\text{hpf}}(\text{nnm})/a_{\text{hpf,av}}(\text{nnm})$.

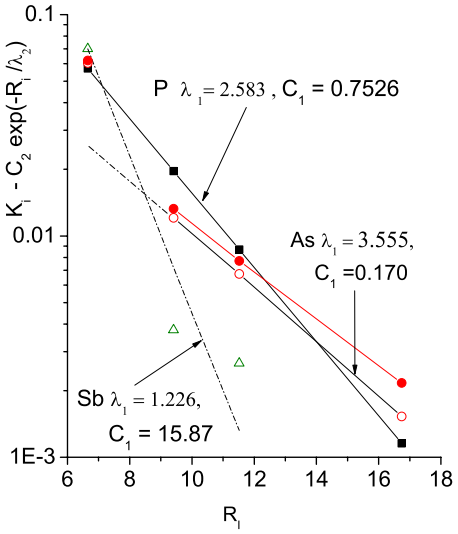

FIG. 2. (Color online) $K_i - C_2 \exp(-R_i/\lambda_2)$ versus R_i. For P (■), a good exponential fit is obtained with $C_1=0.752\,6$ and $\lambda_1=2.583$ Å. For As (○), an exponential was found for only the three distant sites with $\lambda_1=3.55$ Å and calculated value $\Delta a_{\text{hpf}}/a_{\text{hpf,av}}$ for (224) was only half the experimental value. A second curve for a slightly larger value for λ_1 is shown for As from reducing C_2 by 16% because of the energy denominator in Eq. (2). For Sb (△) the dashed line represents a crude exponential ($\lambda_1=1.226$ Å) that yields $(\Delta a_{\text{hpf}}/a_{\text{hpf,av}})_{\text{calc}}$ 40% too large for (444) and 10% too small for (228). The Sb experimental value for (2212) from Table I is zero and the $C_2 \exp(-r/\lambda_2)$ is already too large.

The P-donor results for $\Delta a_{\text{hpf}}/a_{\text{hpf,av}})_{\text{calc}}$ in Table II are in very good agreement with the experimental values obtained from Table I. The rms deviation is 0.077 with the largest deviation arising from the (444) inversion-related pair. The IM rms deviation is more than ten times larger with most of the deviation coming from (224) and (444). Fitting the data with a single term $C_1 \exp(-R_i/\lambda_1)$ in ψ_{tet} will provide a much poorer fit that is unsatisfactory. The results strongly support two terms in $V_{\text{tet}}(\mathbf{r})$: the first from the nn dipoles and the second much smaller term ($C_1/C_2 \sim 42$) from the more distant second and third nn dipoles. The ratio $\lambda_2/\lambda_1=4.14$ supports this interpretation.

The treatment of the As and Sb donors is more difficult than for P because the valence-band bonding orbital for the nn bond is composed of four (s, p) [As] and five (s, p) [Sb], respectively. However, the second and third nn bonds are Si

TABLE II. P-donor fitting parameters and calculated and experimental results. $C_1=0.752\,6$, $\lambda_1=2.583$ Å, $C_2=0.017\,81$, and $\lambda_2=10.7$ Å.

Site	R_{nnm} (Å)	$[\,]_{\text{KL}}/[\,]_{\text{is}}$	$C_1 \exp(-R_i/\lambda_1)$	$(\Delta a_{\text{hpf}}/a_{\text{hpf,av}})_{\text{IM}}$	$(\Delta a_{\text{hpf}}/a_{\text{hpf,av}})_{\text{calc}}$	$(\Delta a_{\text{hpf}}/a_{\text{hpf,av}})_{\text{expt}}$
(224)	6.6504	0.765	0.0571	0.130	0.0510	0.0503
(444)	9.4054	1.134	0.0197	0.188	0.123	0.1414
(228)	11.5188	1.249	0.00868	0.0275	0.0368	0.0341
(2212)	16.7364	2.049	0.00116	0.0215	0.0300	0.0297

TABLE III. As donor fitting parameters and calculated and experimental results. $C_1=0.017\,0$ and $\lambda_1=3.555$ Å.

Site	R_i	$[\,]_{KL}/[\,]_{is}$	$C_1\exp(-R_i/\lambda_1)$	$(\Delta a_{hpf}/a_{hpf,av})_{IM}$	$(\Delta a_{hpf}/a_{hpf,av})_{calc}$	$(\Delta a_{hpf}/a_{hpf,av})_{expt}$
(224)	See	0.676	0.02621	0.135	0.0242	0.0474
(444)	Table	1.033	0.01208	0.196	0.0805	0.0805
(228)	II	1.2156	0.006733	0.0298	0.0311	0.0311
(2212)		2.2204	0.00153	0.0246	0.0350	0.0351

bonds and it is plausible to assume that the second term $C_2\exp(-R_i/\lambda_2)$ in ψ_{tet} will be nearly the same as for P. This assumes the radial electric field E_r is the same for all donors for $r>4$ Å because central-cell effects are negligible at this r and $E_r=e/\varepsilon_h r^2$.This allows a direct determination of $C_1\exp(-R_i/\lambda_1)$ from $K_i-C_2\exp(-R_i/\lambda_2)$. Table III shows the fit for the Si:As.

One obtains a very good fit for the three more distant sites but with $\lambda_1=3.555$ □ and $C_1=0.1702$. With these values, one obtains a calculated value for (224) one half that of the experimental value. The rms deviation is 1.21 for As with nearly all the deviation from (224), but this is a factor of 5 smaller than the IM rms deviation. One cannot explain all the As inversion-related sites with the two term expression $C_1\exp(-R_i/\lambda_1)+C_2\exp(-R_i/\lambda_2)$. The meaning of the 38% increase in λ_1 for As must be related to the nn covalent bond involving Si (3*s*, 3*p*) orbitals and As (4*s*, 4*p*) orbitals. If the dipoles move outward 38%, this could account for the difference in λ_1. However, one must account for the much smaller C_1 and the need for an extra term for just the (224) site. If one employed the P result $C_1\exp(-R_i/\lambda_1)$ for the (224) site for As the calculated result $(\Delta a_{hpf}/a_{hpf,av})_{calc}$ would be only 5% too small, but one would have to explain why the first term $C_1\exp(-R_i/\lambda_1)$ could be characterized by two different λ_1 values.

The same fitting procedure for the Sb donor is less satisfactory. Using the same approach as for As, one cannot find a first term characterized by a single λ_1. This is illustrated in Fig. 2 showing $K_i-C_2\exp(-R_i/\lambda_2)$ versus R_i. The best that one can do is choose an average slope [$\lambda_{1,av}\sim 1.226$ Å and $C_1=15.87$], leading to a substantial overestimate (48%) for (444) and an underestimate (10%) for (228). If one chooses the much flatter curve based on only (444) and (228) one finds $(\Delta a_{hpf}/a_{hpf,av})_{calc}$ a factor of 5.2 too small for (224) and (2212) would be much too large. This choice with such a large λ_1 seems implausible. It is worth recalling that Sb seems to be the most anomalous donor. Despite the poorer fit for Sb, the IM calculated results (Table IV) are much worse than the present results, particularly, for (224) and (444). The small Sb experimental value for (2212) is certainly a problem that the IM and present calculations do not resolve. For both P and As the (2212), experimental value is close to the (228) experimental value.

The experimental donor anomalies $(\Delta a_{hpf}/a_{hpf,av})$ for (224) are Sb>P>As, for (444) are P>As>Sb, for (228) are P>As>Sb, and for (2212) are As>P>Sb; although the As-P difference is within the experimental errors for (228) and (2212). The normal donor anomaly based on donor binding energy is As>P>Sb. The smaller values for As are consistent with the energy denominator $(E_{1S\text{-}A1}-E_{n,\ell=3,m=\pm 2})$ in Eq. (2). The calculated IM values for Δa_{hpf} have the normal donor anomaly with As>P>Sb.

VI. DISCUSSION

The electrostatic potential from the four nn dipoles is given by $(1/\varepsilon_h)\Sigma_{i=1}^{4}\mathbf{p}_i\cdot(\mathbf{r}-\mathbf{r}_i)/|\mathbf{r}-\mathbf{r}_i|^3$, where $\mathbf{r}$ is measured from the donor origin and $\mathbf{r}_i$ is the position of the *i*th dipole [$\mathbf{r}_i=\mathbf{d}_i/2$, $i=1$ to 4]. This φ_{4d} includes the tetrahedral component V_{tet} and a non-Coulombic spherical component $V_{sph}(r)$. $V_{tet}(r)$ falls off as r^{-4} for $r>|\mathbf{r}_i|$ characteristic of an octupole moment, while for $r<\frac{1}{2}|\mathbf{r}_i|$ $V_{tet}(r)\propto r$. V_{tet} is of the opposite sign in these two regimes but is positive for $r>|\mathbf{r}_i|$. $V_{sph}(r)\propto r^{-5}$ for $r>|\mathbf{r}_i|$ but $V_{sph}(r\to 0)\to -2.30\ p_i/|\mathbf{r}_i|^2$. $V_{sph}(r\to 0)$ also changes sign between $r>|\mathbf{r}_i|$ and $r<|\mathbf{r}_i|$. Since the four $\mathbf{p}_i$ are aligned along the $\mathbf{d}_i$, one has $\Sigma_i^4\mathbf{p}_i=0$ and there is no dipolar field at $r\gg|\mathbf{r}_i|$ and the large r potential is dominated by V_{tet}. Nevertheless, $V_{tet}(\mathbf{r})$ is a short-range potential and the negative portion for $r<|\mathbf{r}_i|$ makes a negligible contribution to the matrix elements $\langle\psi_{n,\ \ell=3,\ m=\pm 2}|V_{tet}(\mathbf{r})|\psi_{d,GS}\rangle$. A rough estimate of the GS energy correction from $V_{tet}(\mathbf{r})$ can be made employing $V_t=39.3\ \text{eV}\times L^4$ (L in Å), the single valley $\psi_{GS}=(\pi b^{*3})^{-1/2}e^{-r/b^*}$, and ψ_{tet} in Eq. (6). The result for Si:P is $\delta E_{GS}=-0.017$ meV. Most of the result comes for the nn

TABLE IV. Sb donor fitting parameters and calculated and experimental results. $C_1=15.87$ and $\lambda_1=1.226$ Å.

Site	R_i	$[\,]_{KL}/[\,]_{is}$	$C_1\exp(-R_i/\lambda_1)$	$(\Delta a_{hpf}/a_{hpf,av})_{IM}$	$(\Delta a_{hpf}/a_{hpf,av})_{calc}$	$(\Delta a_{hpf}/a_{hpf,av})_{expt}$
(224)	See	0.788	0.0699	0.137	0.0627	0.0627
(444)	Table	1.077	0.00376	0.184	0.0708	0.048
(228)	II	1.261	0.00265	0.027	0.0201	0.022
(2212)		2.041	0.00108	0.024	0.0230	0.00 (?)

TABLE V. Magnitude of V_{tet} and $E_{\text{tet-max, }r}$.

R (Å)	$V_{\text{tet}}(R)$ (eV)	$E_{\text{tet-max, }r}$ (kV/cm)	$E_{\text{Coul, }r}$ (kV/cm)
2.351	0.1135	1.93×10^{4}	2.10×10^{4}
9.4047	0.00039	1.88×10^{1}	1.31×10^{3}

dipoles for $r>b$. Ning and Sah[5] stated there would be no correction to the GS energy from $V_{\text{tet}}(\mathbf{r})$, but this is because they did not consider the ψ_{tet} contribution to ψ_{GS}.

The contribution of the second and third nn dipoles involves a sum over 12 dipoles for each case. $\mathbf{E}\cdot\mathbf{d}_i = E_r d\cos\theta$ and $\cos\theta=0.685$ and 0.889 for second and third nn. Even though further away the third nn dipoles are important because they are closer to the radial direction $\mathbf{r}$ and the 3 $\mathbf{p}_i$ in the positive octant point in the same direction as the nn $\mathbf{p}_1$. The P-donor results yield $\lambda_2/\lambda_1=4.14$ in good agreement with $|\mathbf{r}_i|_{3\text{rdnn}}/|\mathbf{r}_i|_{\text{nn}}=4.128$, from which one might infer the second nn dipoles are not important. However, $E_{r\ 2\text{nn}}/E_{r\ 3\text{nn}}\sim 2.7$ and a detailed analysis suggests the contribution of the second and third nn dipoles might be comparable. An accurate estimate of the ratio C_2/C_1 (0.0236 for P) is difficult to calculate from first principles.

From $\varphi_{4d,\text{tet}}(x=y=z)/p$ in Fig. 1, one can estimate the magnitude of V_{tet} using $p=0.142\ e\gamma d=4.69\times10^{-11}e$ Coulomb meter for Si:P. The magnitudes of V_{tet}, $E_{\text{tet-max, }r}$, and $E_{\text{Coul, }r}$ at two values of R are in Table V. The results show that V_{tet} is about one half of $V_{\text{Coul}}=e^2/\varepsilon_h r$ at the nn (111) site but is down by a factor of 300 at (444). $E_{\text{tet-max, }r}=-\partial V_{\text{tet}}/\partial r|_R$ is nearly equal to the Coulomb field $E_{\text{Coul},r}$ at $R=2.351$ Å, however both V_{tet} and $E_{\text{tet-max, }r}$ are short range (r^{-4} and r^{-5}, respectively). The negative part of $V_{\text{tet}}(x=y=z)$ for $r<1$ Å has a negligible effect on the matrix elements [Eq. (4)] and ψ_{tet}. However, the spherical portion of $\varphi_{4d}(r)$ becomes large and repulsive as $r\to0$ and might have some affect on ψ_{KL}.

The role of P donors in Si as qubits near metal gates connected with quantum computer architecture has generated significant interest in the Stark effect arising from a uniform external electric field. Stark effect calculations[15–17] add a linear term $-eEz$ to the Hamiltonian. There is a critical field E_c involved. Martins *et al.*[15] found $E_c\propto 1/Z_B$ [Z_B the distance to the metal gate] and for $Z_B=10.86$ nm ($Z_B\approx5a^*$) find $E_c\sim53$ kV/cm. Friesen[16] and Debernardi *et al.*[17] for $Z_B\to\infty$ found $E_c\sim37$ kV/cm and 24.5 kV/cm, respectively. These values are still much less than $E_{\text{Coul, }r}$ at both the nn and third nn valence bond orbitals. A linear $\mathbf{E}$ field along (001) will split the ENDOR shells O and H (as well as others). For shell O the quartet (444), ($\underline{4}44$), ($4\underline{4}4$), and ($44\underline{4}$) will split into two doublets [(444), ($\underline{4}\underline{4}4$) and ($\underline{4}4\underline{4}$), ($4\underline{4}\underline{4}$)]. Debernardi *et al.*[17] calculated the splitting of shell A and found $a_{\text{hpf}}(00\underline{4})-a_{\text{hpf}}(004)=93$ kHz at $E=10$ kV/cm which might be observable. Bradbury *et al.*[18] reported a hyperfine shift $\Delta a/a=3.7\times10^{-5}$ cm^2/kV$^2\times E^2$ for ^{121}Sb implanted in a ^{28}Si epilayer which is a factor of 4 larger than the calculated shell A results for Si:P in. With the exception of the Si donor ENDOR data, it is not yet clear how or whether $V_{\text{tet}}(\mathbf{r})$ and $\psi_{\text{tet}}(\mathbf{r})$ will affect the external electric-field Stark effect.

The electric octupole moment is $O_{xyz}=e\int xyz|\psi_d|^2dV\approx -2e\int xyz\psi_{\text{KL}}\psi_{\text{tet}}dV$ of the donor charge distribution. For an estimate, one employs $\psi_{\text{KL}}=(\pi b^{*3})\exp(-r/b^*)$ and after the angular integration have

$$O_{xyz}=-(8\pi e/105)\int r^8dr\{C_1\exp[-r(1/\lambda_1+1/b^*)] + C_2\exp[-r(1/\lambda_2+1/b^*)]\}. \quad (9)$$

For P this yields $O_{xyz}/e=-[1.967\times10^3C_1+2.411\times10^6C_2]$ Å^3. The second term is 30 times the first term for $C_2/C_1=0.023\ 6$. This result corresponds to a giant octupole moment which is very much larger than that for CF_4, but it occurs in a very dilute system with an average donor spacing of 10^3 Å. In liquid and solid CF_4 (Ref. 19) and also solid SnI_4 (Ref. 20) octupole-octupole interactions can affect the thermodynamic properties. The giant octupole results from the second and third nn electric dipoles.

The origin of V_{tet} originates from the $\mathbf{E}$-field-induced dipoles at the nn, second nn, and third nn covalent bonds. This V_{tet} introduces $\psi_{\text{tet}}=-(xyx/a^3)[C_1\exp(-r/\lambda_1)+C_2\exp(-r/\lambda_2)]$ which allows an excellent fitting analysis for the P donor, a reasonable fitting analysis for the As donor and a less satisfactory result for Sb. This is accomplished without the $F_{xi}\sin k_0X_i$ terms in Eq. (46) in IM. These terms appeared because $u_n(\mathbf{k},\mathbf{r})$ was complex off the $\Gamma\Delta X$ axis. However, if we start with Eq. (11) in IM and employ $u_n(\mathbf{k},\mathbf{r})=|u_n(\mathbf{k},\mathbf{r})|\exp(i\varphi_n(\mathbf{k})$ where $\varphi_n(\mathbf{k})$ is a k-dependent phase angle for the nth band. Equation (15) in IM becomes

$$[E_n(\mathbf{k})-E_{\text{GS}}]A_n(\mathbf{k})=-\langle u_n(\mathbf{k},\mathbf{r})^*|U(r)|\psi_{\text{KL}}\rangle, \quad (10)$$

where $U(r)$ in IM was chosen positive. $An(\mathbf{k})\propto\exp[-i\varphi n(\mathbf{k})]$, but of most importance the product $A_n(\mathbf{k})u_n(\mathbf{k},\mathbf{r})$ is real. Hence the IM Eq. (11) can be written $\psi_d=\Sigma_{n\mathbf{k}}|A_n(\mathbf{k})||u_n(\mathbf{k},\mathbf{r})|\exp(i\mathbf{k}\cdot\mathbf{r})$ and with this equivalent result one observes that one can arbitrarily choose a real $|u_n(\mathbf{k},\mathbf{r})|$ and a real $|A_n(\mathbf{k})|$ and with this definition of ψ_d, one will not obtain the $F^I_{xi}\sin k_0X_i$ terms found in Eq. (46) in IM. This situation was first pointed out in CA (Ref. 4) in Ref. 45. Even without these $F^I_{xi}\sin k_0X_i$ terms, IM still found a LOIS for ψ_d. However, it is not clear that one can obtain such a result with a purely spherical $U(r)$. A key approximation of KL EM theory is the use of $u_n(\mathbf{k}_m,\mathbf{r})$ in the Bloch function $\psi_n(\mathbf{k},\mathbf{r})$ in the vicinity of the minimum at $\mathbf{k}_m$. Calculations in IM for Re$[u_n(\mathbf{k},\mathbf{r})]$ for the first and second conduction bands (see Figs. 19 and 20 in IM) suggesting this approximation is rather good; although corrections might be required as ψ_d becomes much more accurate. The symmetry operations 2_z [$x\to-x$, $y\to-y$, and $z\to z$] and S_4 [$x\to y$, $y\to-x$, and $z\to-z$] of the tetrahedral group T_d yield 2_z $\psi_{\text{tet}}=\psi_{\text{tet}}$ and S_4 $\psi_{\text{tet}}=\psi_{\text{tet}}$, verifying ψ_{tet} belongs to the A_1 representation of the T_d group. On the other hand, for $\delta\psi=F^I_x\sin k_0x+F^I_y\sin k_0y+F^I_z\sin k_0z$ from Eq. (46) in IM, one finds 2_z $\delta\psi\neq\delta\psi$ suggesting this $\delta\psi$ does not belong to the A_1 representation. This raises serious questions about the IM sum of sine terms in their Eq. (46).

Pantelides[21] gave a comprehensive review of the theory of impurities and defects in semiconductors including EMT,

central-cell corrections, and other theoretical approaches but did not discuss $V_{\text{tet}}(\mathbf{r})$ or the ENDOR data, although the IM paper is referenced. As shown herein, it is precisely the HM ENDOR data and the LOIS pairs identified by IM that provide the motivation for $V_{\text{tet}}(\mathbf{r})$ and $\psi_{\text{tet}}(\mathbf{r})$. Future theoretical work needs to explore the consequences of $V_{\text{tet}}(\mathbf{r})$ on the properties of substitutional impurities.

VII. CONCLUSIONS

The tetrahedral potentials responsible for ψ_{tet} are shown to arise not from point charges but from **E**-field-induced electric dipoles associated with first nn, second nn, and third nn covalent bonds as treated by Harrison. This is a general result and will apply to all substitutional impurities with T_d symmetry in diamondlike and zinc-blende semiconductors. At large r ($r \gg b$), the potential $\Sigma_{i=1}^{4} \mathbf{p}_i \cdot (\mathbf{r}-\mathbf{r}_i)/|r-r_i|^3$ from four dipoles produces V_{tet} at $r > |\mathbf{r}_i|$. Since $\Sigma_{i=1}^{4} \mathbf{p}_i = 0$ the four dipoles produce an octupole moment for $r \gg b$ consistent with V_{tet}. $\psi_{\text{tet}} = -(xyx/a^3)[C_1 \exp(-r/\lambda_1) + C_2 \exp(-r/\lambda_2)]$ is consistent with the A_1 representation and the four experimental values of $(\Delta a_{\text{hpf}}/a_{\text{hpf,av}})$ permit an excellent fit for P, a reasonable fit for As, and a less satisfactory fit for Sb. This fit is better than the calculated values of IM. Theoretical reasons are given why the IM component of ψ_d, namely, $F_x^I \sin k_0 x + F_y^I \sin k_0 y + F_z^I \sin k_0 z$ is not consistent with the A_1 representation. Although $V_{\text{tet}}(\mathbf{r})$ has a negligible effect on GS energy the $\psi_{\text{tet}}(\mathbf{r})$ component of ψ_d accounts reasonably well for the lack-of-inversion symmetry as measured and the inversion-related shells $[M, L]$, $[H, O]$, $[I, P]$, and $[S, T]$ identified by Ivey and Mieher with the specific lattice sites. This work would not have been possible without this identification of specific lattice sites for the inversion-related pairs with the experimental shells. Future work should examine what effects V_{tet} and ψ_{tet} might have on the external Stark effect.

ACKNOWLEDGMENT

The author thanks E. B. Hale for useful suggestions on the manuscript.

[1] W. Kohn, in *Solid State Physics*, edited by Seitz and Turnbull (Academic, New York 1957), Vol. 5.
[2] R. L. Aggarwal and A. K. Ramdas, Phys. Rev. **140**, A1246 (1965).
[3] R. A. Faulkner, Phys. Rev. **184**, 713 (1969).
[4] T. G. Castner, Phys. Rev. B **2**, 4911 (1970).
[5] T. H. Ning and C. T. Sah, Phys. Rev. B **4**, 3468 (1971).
[6] E. B. Hale and R. L. Mieher, Phys. Rev. **184**, 739 (1969).
[7] J. L. Ivey and R. L. Mieher, Phys. Rev. B **11**, 822 (1975).
[8] B. E. Kane, Nature (London) **393**, 133 (1998).
[9] D. R. McCamey, H. Huebl, and M. S. Brandt, W. D. Hutchinson, J. C. McCallum, R. G. Clark, and A. R. Hamilton, Appl. Phys. Lett. **89**, 182115 (2006).
[10] A. De, C. E. Pryor, and M. E. Flatte, Phys. Rev. Lett. **102**, 017603 (2009).
[11] I. Zutic, J. Fabian, and S. Das Sarma, Rev. Mod. Phys. **76**, 323 (2004).
[12] W. A. Harrison, *Electronic Structure and the Properties of Solids* (W. H. Freeman, San Francisco, 1980) p. 120.
[13] L. I. Schiff, *Quantum Mechanics* (McGraw-Hill, NYC, 1949) p. 85, Eq. (16.21); The sum $\Sigma_{q=7}^{7} L_q^7(\rho) s^q/q! = [s^7/(1-s)^8]\exp[-\rho s/(1-s)]$ where a -1 has been removed for $L_{n+x}^{2\ell+1}(\rho)$ in Eq. (16.22). For the empirically obtained $\lambda_1 = 2.583$ Å and $4a_{\text{EM}}^* = 80.716$ Å, $s = 0.9687$, $(1-s) = 0.031\,3$, and $s/(1-s) \approx 31.0$. The key to the result is that the sum yields a single exponential characterized by a length scale $\ll 4a_{\text{EM}}^*$.
[14] T. G. Castner, Phys. Rev. B **77**, 205208 (2008).
[15] A. S. Martins, R. B. Capaz, and B. Koiller, Phys. Rev. B **69**, 085320 (2004).
[16] M. Friesen, Phys. Rev. Lett. **94**, 186403 (2005).
[17] A. Debernardi, A. Baldereschi, and M. Fanciulli, Phys. Rev. B **74**, 035202 (2006).
[18] F. R. Bradbury, A. M. Tyryshkin, G. Sabouret, J. Bokor, T. Schenkel, and S. A. Lyon, Phys. Rev. Lett. **97**, 176404 (2006).
[19] H. Enokido, T. Shinoda, and Y. Mashiko, Bull. Chem. Soc. Jpn. **42**, 3415 (1969).
[20] K. Fuchizaki and K. Nagai, Solid State Commun. **132**, 305 (2004).
[21] S. Pantelides, Rev. Mod. Phys. **50**, 797 (1978).